nature genetics

Loss of *ACTN3* gene function alters mouse muscle metabolism and shows evidence of positive selection in humans

Daniel G MacArthur[1,2], Jane T Seto[1,2], Joanna M Raftery[1], Kate G Quinlan[1,2], Gavin A Huttley[3], Jeff W Hook[4], Frances A Lemckert[4], Anthony J Kee[5], Michael R Edwards[6], Yemima Berman[1], Edna C Hardeman[5], Peter W Gunning[2,4], Simon Easteal[3], Nan Yang[1] & Kathryn N North[1,2]

More than a billion humans worldwide are predicted to be completely deficient in the fast skeletal muscle fiber protein α-actinin-3 owing to homozygosity for a premature stop codon polymorphism, R577X, in the *ACTN3* gene. The R577X polymorphism is associated with elite athlete status and human muscle performance, suggesting that α-actinin-3 deficiency influences the function of fast muscle fibers. Here we show that loss of α-actinin-3 expression in a knockout mouse model results in a shift in muscle metabolism toward the more efficient aerobic pathway and an increase in intrinsic endurance performance. In addition, we demonstrate that the genomic region surrounding the 577X null allele shows low levels of genetic variation and recombination in individuals of European and East Asian descent, consistent with strong, recent positive selection. We propose that the 577X allele has been positively selected in some human populations owing to its effect on skeletal muscle metabolism.

The α-actinins are an ancient family of actin-binding proteins. Of the four mammalian α-actinins, α-actinin-3 is the most specialized, with expression restricted largely to the fast glycolytic skeletal muscle fibers[1] that are responsible for rapid force generation. Notably, α-actinin-3 is absent in ~18% of healthy individuals of European descent owing to homozygosity for a common nonsense polymorphism in the *ACTN3* gene, R577X[2]. The frequency of the 577X null allele differs between human groups: it is ~10% in Africans but approaches 50% in Eurasian populations[1]. Two independent studies have reported associations between R577X and elite athlete status[3,4]; the frequency of the 577XX null genotype is lower in sprinting and power athletes and higher in endurance athletes. The 577XX genotype has also been associated with lower muscle strength[5] and poorer sprint performance[6] in two large studies of non-athletes. The mechanism(s) by which α-actinin-3 deficiency influences muscle function remain unclear.

To characterize the phenotypic consequences of α-actinin-3 deficiency, we have generated an *Actn3* knockout mouse line (**Fig. 1a**). Homozygous knockout (*Actn3*$^{-/-}$) mice do not express any detectable α-actinin-3 protein, as assessed by either immunohistochemistry or immunoblotting (**Fig. 1b**,**c**). *Actn3*$^{-/-}$ mice were morphologically similar to wild-type (*Actn3*$^{+/+}$) littermates, they showed normal sarcomere formation at the light and electron microscope level and they did not demonstrate substantial loss of fast glycolytic (2B) fibers (data not shown). Loss of α-actinin-3 in fast fibers seems to be compensated for by an upregulation of the related protein α-actinin-2 (**Fig. 1c**), which shifts from preferential expression in oxidative fibers to uniform staining in all fibers in *Actn3*$^{-/-}$ muscle (**Fig. 1b**). The *Actn3*$^{-/-}$ mouse thus mimics α-actinin expression in 577XX humans, who also show α-actinin-3 deficiency and α-actinin-2 expression in all muscle fibers[1].

Given the differing frequencies of the 577XX genotype in elite sprint and endurance athletes, we investigated whether the loss of α-actinin-3 altered skeletal muscle metabolism. We found that muscle sections from *Actn3*$^{-/-}$ mice showed more intense staining than those from *Actn3*$^{+/+}$ mice for two markers of aerobic metabolism, NADH-tetrazolium reductase (NADH-TR) and succinate dehydrogenase (SDH) (**Fig. 2a**). Quantitative analysis showed a significant ($P < 0.02$) increase in regions staining positively for NADH-TR in *Actn3*$^{-/-}$ muscle compared to *Actn3*$^{+/+}$ muscle. Immunohistochemical analysis with myosin heavy chain 2B, a marker of fast glycolytic fibers, indicated that the increase in oxidative enzyme activity does not result from a loss of fast fibers but rather from altered metabolism in these fibers (**Fig. 2b**). Two mitochondrial markers (cytochrome c oxidase and

[1]Institute for Neuromuscular Research, Children's Hospital at Westmead, Sydney, New South Wales 2145, Australia. [2]Discipline of Paediatrics and Child Health, Faculty of Medicine, University of Sydney, Sydney, New South Wales 2006, Australia. [3]John Curtin School of Medical Research, The Australian National University, Canberra, Australian Capital Territory 0200, Australia. [4]Oncology Research Unit, Children's Hospital at Westmead, Sydney, New South Wales 2145, Australia. [5]Muscle Development Unit, Children's Medical Research Institute, Sydney, New South Wales 2145, Australia. [6]Biotechnology and Biomolecular Sciences, University of New South Wales, Sydney, New South Wales 2052, Australia. Correspondence should be addressed to K.N. (kathryn@chw.edu.au).

Received 16 January; accepted 7 August; published online 9 September 2007; doi:10.1038/ng2122

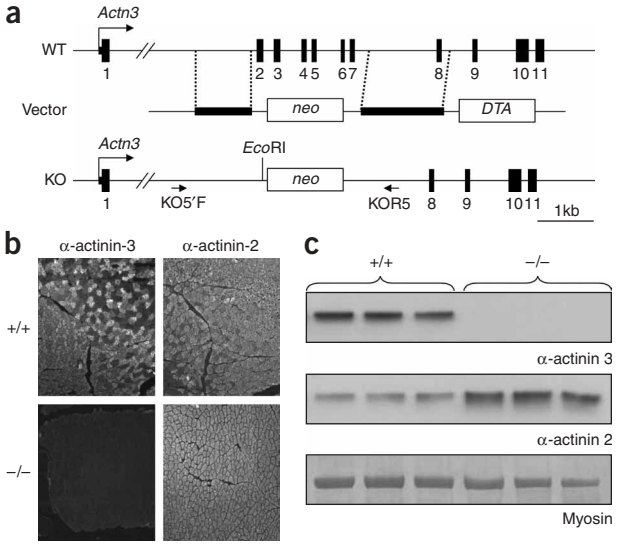

Figure 1 Generation and analysis of *Actn3*$^{-/-}$ mice. (**a**) Generation of the *Actn3* knockout locus. Homologous recombination in *Actn3*$^{+/+}$ embryonic stem cells results in replacement of *Actn3* exons 2–7 with the *neo* marker. (**b**) Immunohistochemistry for the sarcomeric α-actinins in *Actn3*$^{+/+}$ and *Actn3*$^{-/-}$ mice, showing loss of α-actinin-3 and altered expression pattern of α-actinin-2 in *Actn3*$^{-/-}$ muscle. (**c**) Immunoblot analysis shows absent α-actinin-3 and upregulated α-actinin-2 in *Actn3*$^{-/-}$ mice compared to *Actn3*$^{+/+}$ littermates. Total myosin is shown as a loading control.

mitochondrial porin) were upregulated in the muscle of *Actn3*$^{-/-}$ mice (**Fig. 3a**), consistent with increased mitochondrial density in *Actn3*$^{-/-}$ muscle.

As further confirmation of these metabolic findings, we analyzed the activity of two key enzymes involved in pyruvate metabolism (**Fig. 3b**). Pyruvate, the end metabolite of the glycolytic pathway, represents a branch point in muscle metabolism: in fast muscle fibers it is predominantly converted to lactate by the anaerobic pathway enzyme lactate dehydrogenase (LDH), and in slow fibers it is preferentially oxidized within the mitochondria, a slower but more efficient process in which citrate synthase catalyses the first reaction. The activity of LDH was 16% lower ($P < 0.001$) and that of citrate synthase was 22% higher ($P < 0.05$) in *Actn3*$^{-/-}$ mice compared to *Actn3*$^{+/+}$ controls. These results indicate that the loss of α-actinin-3 results in a significant shift in the metabolic pathways of fast muscle fibers away from their typical reliance on the anaerobic lactate pathway toward the slower but more efficient aerobic pathway normally associated with slow muscle fibers.

To determine if this alteration in skeletal muscle metabolism influences endurance performance, we subjected *Actn3*$^{-/-}$ mice and *Actn3*$^{+/+}$ littermate controls to a modified version of the intrinsic exercise capacity test, in which mice were run on a motorized treadmill at increasing speeds until they reached exhaustion. *Actn3*$^{-/-}$ mice performed significantly better than *Actn3*$^{+/+}$ mice in this test, running on average 33% further than their *Actn3*$^{+/+}$ littermates before reaching exhaustion (**Fig. 3c**). These findings suggest that the shift toward oxidative metabolism observed in the muscle of *Actn3*$^{-/-}$ mice increases intrinsic endurance performance, consistent with the overrepresentation of the 577XX null genotype in elite female endurance athletes[3].

The phenotypic changes associated with α-actinin-3 deficiency in mice, coupled with the association of the 577X allele with reduced sprint and increased endurance performance, suggest that the 577X allele also influences muscle metabolism in humans. This in turn raises the possibility that the high frequency of 577X in some human populations has resulted from historical natural selection for increased metabolic efficiency. To investigate this possibility, we sequenced a 3.7-kb region of genomic DNA, centered on R577X, in 96 DNA samples previously analyzed by the International HapMap Project[7] (**Supplementary Table 1** online), using primers described in **Supplementary Table 2** online. Our cohort included 32 Utah residents with ancestry from northern and western Europe (CEU), 32 Yoruba from Ibadan, Nigeria (YRI), 16 Han Chinese from Beijing (CHB) and 16 Japanese from Tokyo (JPT). The 32 CHB and JPT samples were grouped into a single cohort, designated ASN. For comparison, this region was also sequenced from a single chimpanzee.

Within our cohorts, we found frequencies of the 577X null allele similar to those reported previously[1]: 0.55 in CEU, 0.52 in ASN and 0.09 in the African YRI cohort. Owing to the low population frequency of the 577X allele in the YRI cohort, we restricted further analyses to the 64 Eurasian (CEU+ASN) samples. The sequenced region in the CEU+ASN cohorts contains 21 SNPs, including five missense polymorphisms and the R577X nonsense SNP, and one three base-pair indel (**Supplementary Table 3** online). These polymorphisms resolve into 12 haplotypes in three major haplogroups (**Fig. 4a**) of which two (R1 and R2) carry the 577R allele, and the third (X) carries the 577X allele. A long branch separates the X haplogroup from the relatively closely related R1 and R2 clusters. An excess of nonsynonymous substitutions associated with this branch is consistent with relaxed selective constraint specific to the lineage carrying the 577X alteration.

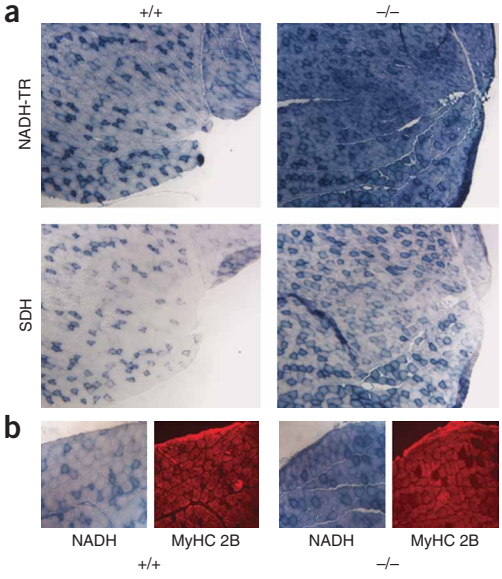

Figure 2 Fast muscle fibers in *Actn3*$^{-/-}$ mice show increased staining for markers of aerobic metabolism. (**a**) Representative images of quadriceps muscle sections show increased staining for NADH-tetrazolium reductase (NADH-TR) and succinate dehydrogenase (SDH) in *Actn3*$^{-/-}$ muscle compared to *Actn3*$^{+/+}$ mice. (**b**) Higher-power images of serial sections stained for myosin heavy chain (MyHC) 2B and NADH show that fast glycolytic (2B-positive) fibers stain more darkly for NADH-TR in *Actn3*$^{-/-}$ muscle.

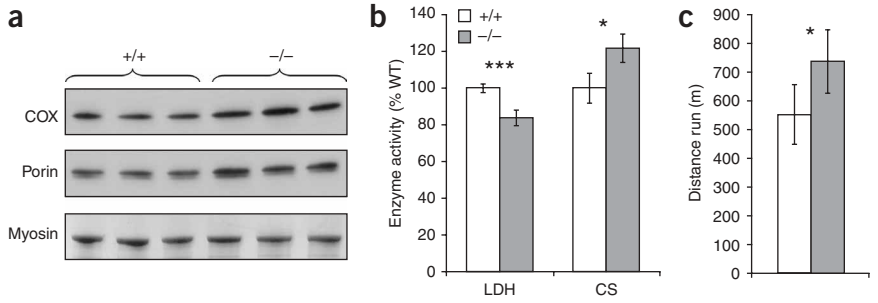

Figure 3 *Actn3*$^{-/-}$ muscle shows increased expression of mitochondrial markers, altered metabolic enzyme activity and increased endurance capacity. (**a**) Immunoblot analysis shows increased expression of the mitochondrial markers cytochrome c oxidase (COX) and mitochondrial porin in *Actn3*$^{-/-}$ mice compared to *Actn3*$^{+/+}$ littermates. Total myosin is shown as a loading control. (**b**) *Actn3*$^{-/-}$ mice show decreased lactate dehydrogenase (LDH) activity and increased citrate synthase (CS) activity compared to *Actn3*$^{+/+}$ (WT) littermates. Data were collected from seven *Actn3*$^{+/+}$ and seven *Actn3*$^{-/-}$ muscle lysates. For each enzyme, mean *Actn3*$^{+/+}$ activity is set to 100%. (**c**) Total distance run before exhaustion in an intrinsic exercise capacity test by 20 *Actn3*$^{+/+}$ and 23 *Actn3*$^{-/-}$ mice. In **b** and **c**, error bars indicate 95% c.i. * $P < 0.05$, *** $P < 0.001$.

Although this increased substitution rate makes precise dating difficult, the length of the branch separating 577X haplotypes from the inferred ancestral sequence and the presence of the 577X allele in all studied human populations[1] suggest the 577X substitution preceded the appearance of anatomically modern humans in Europe and Asia 40,000–60,000 years ago (40–60 kya). Notably, despite the apparent age, high frequency and relaxed selective constraint associated with the 577X allele, the 577X haplogroup contains little variation. In the CEU sample, we did not observe any variation among 35 577X haplotypes, and in the ASN cohort, we observed only three low-frequency polymorphisms on 5/33 577X haplotypes. This low level of variation suggests that the 577X allele achieved its current Eurasian frequency of ~0.5 in a comparatively recent and rapid expansion.

To determine whether this expansion was driven by positive natural selection, we examined the pattern of long-range linkage disequilibrium (LD) surrounding R577X using SNP genotype data from the HapMap project[7]. We employed a conservative algorithmic approach (see Methods) to determine the length of the unbroken long-range haplotype carrying a particular allele, which we refer to as the length of complete homozygosity (LCH). Recent positive selection should result in a long LCH associated with the selected allele, relative to allele frequency and local recombination rate.

We determined the LCH for a genome-wide set of >17,000 autosomal SNP alleles matched to 577X for both allele frequency and local recombination rate in the CEU and ASN HapMap cohorts. Demographic forces should affect LD at all autosomal loci equally, whereas positive selection will result in unusually large locus-specific values of long-range LD[8]. In the CEU cohort, the haplotype carrying the 577X allele is associated with a larger LCH (338,148 bp; **Fig. 4b**) than any other region in the comparison set: more than 100 kb longer than the next-largest value, and more than 100 times the median (3,253 bp) (**Fig. 4c**). The LCH for 577X in the ASN cohort (97,927 bp) is less extreme but is still longer than 98.9% of the values in the comparison set. The inferred recombination rate for the 577R allele in this region is substantial (**Fig. 4b**), demonstrating that the extended haplotypes carrying the 577X allele are not simply an artifact of low local recombination rate. The outlier status of the 577X allele in both populations strongly suggests that the haplotype carrying this allele has been subjected to recent positive selection in European and Asian populations.

The LCH in the CEU and ASN cohorts are both asymmetrical with respect to R577X, but they extend in opposite directions (**Fig. 4b**), probably owing to stochastic recombination events during the expansion of the selected haplotype in the two populations. The LCH regions contiguous with R577X overlap for only ~29.5 kb, spanning two genes: *ACTN3* and *CTSF*. In addition, there is an upstream region of ~29 kb in which both CEU and ASN cohorts show complete homozygosity (**Fig. 4b**), although this region is separated from R577X in the CEU cohort by several SNPs with evidence of recombination; this region contains the last 14 exons of the *BBS1* gene and the final exon of the *ZDHHC24* gene. To identify alternative candidates for the target of selection in these regions, we sequenced all coding exons and

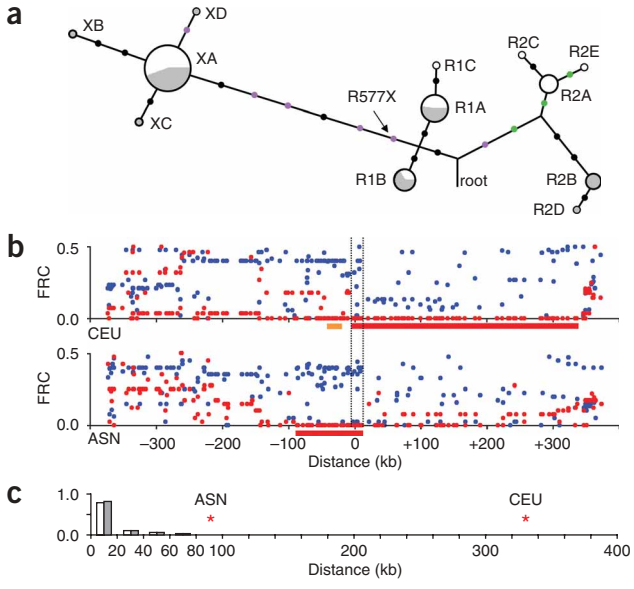

Figure 4 The 577X null allele is associated with low genetic diversity and high long-range LD in Europeans and Asians, suggestive of recent positive selection. (**a**) Haplotype genealogy in CEU and ASN samples. Grey and white circles denote haplotypes, with areas of white and gray proportional to frequency in CEU and ASN cohorts, respectively. Filled circles indicate intronic (black), synonymous (green) and nonsynonymous (purple) mutations. The likely position of the R577X substitution is shown, but note that the precise order of mutations along this branch cannot be inferred. The root of the tree is inferred from the chimpanzee sequence. (**b**) Pattern of long-range LD associated with R577X. The inferred fraction of recombinant chromosomes (FRC) for each HapMap SNP is plotted against physical distance for the 577R (blue) and 577X (red) alleles. Lengths of complete homozygosity (LCH) associated with the 577X allele are shown as red bars. An upstream region of homozygosity shared by ASN and CEU but noncontiguous with R577X is shown in orange. The region of overlap between the contiguous LCH in the two cohorts is shown (dotted lines). (**c**) Distribution of LCH values from a matched genome-wide set of >17,000 SNP alleles in the CEU (white) and ASN (gray) populations. LCH values for 577X in the CEU and ASN cohorts (asterisks) are clear outliers.

proximal splice sites in both areas, excluding exons of the *ACTN3* gene (as any variant in *ACTN3* linked to the sweep would be silenced by the 577X allele), in individuals homozygous for each of the three major haplotype clusters from both the CEU and ASN populations. We identified a total of 15 segregating variants by this analysis, none of which was both putatively functional and linked to the signal of selection (**Supplementary Table 4** online). In addition, we genotyped two previously reported nonsynonymous variants in the *CTSF* gene in 30 CEU and ASN individuals and found them to be monomorphic in these populations. Thus, although we cannot rule out variants in noncoding regions, the best candidate for the target of selection is the 577X allele, which has a known biological effect and which is linked to the signal of selection.

Using a recently described approach[9], we estimate that the sweep in CEU began ~15 kya, whereas in ASN the sweep is considerably older, dating to ~33 kya. The failure of the 577X allele to achieve fixation (that is, failure to reach a frequency of 100%) in either population may simply reflect inadequate time. However, even weak positive selection would be expected to increase the frequency of a beneficial allele to fixation within as little as a few hundred generations[8], substantially less than the estimated age of the 577X allele in the CEU and ASN populations. This may indicate the presence of more complex countervailing or balancing selective pressures acting on the R577X polymorphism and preventing a rapid sweep to fixation within these populations.

In conclusion, we have found that α-actinin-3 deficiency alters skeletal muscle metabolism and increases endurance performance in a knockout mouse model and that the *ACTN3* 577X null allele has been selectively favored in modern humans adapting to the Eurasian environment. We propose that the shift toward more efficient aerobic muscle metabolism associated with α-actinin-3 deficiency underlies the adaptive benefit of the 577X allele and, in turn, potentially explains the overrepresentation of the 577XX genotype among elite endurance athletes[3].

METHODS

Generation of knockout mouse. Figure 1a shows the strategy used to generate a null allele in the mouse *Actn3* gene. We amplified two regions flanking exons 2–7 of the *Actn3* gene using the Expand Long Template PCR system (Roche), with primers containing either *Not*I or *Cla*I restriction sites. These sites were used to clone the two flanking regions into the vector pPGKneoDTA on either side of the neomycin resistance cassette (*neo*).

The linearized vector was electroporated into R1-129 embryonic stem (ES) cells. Screening for the presence of successful homologous recombinants at the *Actn3* locus was performed by amplification with primers KO5′F and KOR5 and digestion with *Eco*RI (**Fig. 1a**). Recombinant ES clones were regrown, injected into cultured BALB/c blastocysts and transferred into pseudopregnant foster mice. Chimeric males identified by brown coat color were bred with 129 females. Heterozygous 129 mice were bred further to produce homozygous knockout mice. Mice were genotyped using by DNA isolated from tail snips, using the same protocol as for ES cells.

All animal experiments were performed in accordance with institutional and Australian National Health and Medical Research (NHMRC) guidelines.

Immunohistochemistry and immunoblotting. Antibodies to the α-actinins were a gift (see Acknowledgments). α-actinin-2 was analyzed using the antibody 4B3 at 1:1,000 for immunohistochemistry (IHC) and 1:200,000 for protein blot, and α-actinin-3 was analyzed using 5B3 at 1:1,000 for IHC and at 1:4,000 for protein blot. IHC for myosin heavy chain 2B was performed using the antibody 10F5, neat. Immunoblotting for mitochondrial porin used the antibody 20B12 (Molecular Probes) at 1:5,000, and immunoblotting for cytochrome c oxidase used 20E8 (Molecular Probes) at 1:2,000. Immunohistochemistry and immunoblotting were performed as described previously[10,11].

Histochemistry. NADH-tetrazolium reductase (NADH-TR) and succinate dehydrogenase (SDH) staining was carried out using standard protocols (**Supplementary Methods** online). Both NADH-TR and SDH stains were performed on sections of whole quadriceps muscle from ten $Actn3^{+/+}$ and ten $Actn3^{-/-}$ mice. In both cases, all $Actn3^{+/+}$ and $Actn3^{-/-}$ mice could be distinguished from one another by two independent observers unaware of their genotype, judging solely from staining intensity and distribution.

Quantitative image analysis of NADH-TR staining was performed on five $Actn3^{+/+}$ and five $Actn3^{-/-}$ male mice using Adobe Photoshop as described in **Supplementary Methods**. Statistical significance was assessed using the Mann-Whitney *U* test in SPSS.

Metabolic enzyme assays. Lactate dehydrogenase (EC 1.1.1.27) and citrate synthase (EC 4.1.3.7) activities were measured spectrophotometrically by modifications of previously described methods[12,13].

Intrinsic exercise capacity test. Mice were tested for intrinsic endurance capacity using a modified version of a previously described protocol[14]. Briefly, 7- to 9-week-old male mice were placed on a motorized treadmill (Columbus Instruments) set at a 15° incline with a baseline speed of 10 m/min. A negative stimulus (a stiff-bristled brush) was placed at the rear of the treadmill. Speed was increased by 1 m/min every 2 min until mice were exhausted, defined as the inability to extricate themselves from the negative stimulus three times within two minutes. Speed and time of exhaustion were recorded, and total distance calculated. All mice were tested by observers unaware of genotype.

Sequencing of R577X region. Ninety-six unrelated DNA samples from the International HapMap Resource were obtained from Coriell Cell Repositories: 32 from CEU (CEPH Utah residents with ancestry from northern and western Europe), 32 YRI (Yoruba from Ibadan, Nigeria), 16 CHB (Han Chinese from Beijing) and 16 JPT (Japanese from Tokyo). A list of the samples used is provided in **Supplementary Table 1**. In addition, the region was sequenced from one chimpanzee DNA sample.

A region of genomic DNA spanning ~3.8 kb (chromosome 11, positions 66082752–66086604 from NCBI build 36.1 of the human genome) centered on the R577X polymorphism (dbSNP rs1815739) was amplified in two overlapping fragments and was fully sequenced using 20 primers (**Supplementary Table 2**). Trace files were trimmed and aligned with a reference sequence using Sequencher (GeneCodes) and manually scanned for polymorphisms. Inference and analysis of haplotypes is described in **Supplementary Methods**.

Long-range LD analysis. Phase 2 genotype data from the CEU and ASN cohorts were downloaded from the HapMap website and were filtered to generate a set of all autosomal SNP alleles with frequencies within 10% of the frequency of 577X and local deCODE estimated recombination rates[15] within 0.05 cM/Mb of the estimated recombination rate of the R577X region. This matched data set contained 17,004 alleles for the CEU cohort and 17,051 alleles for ASN. Because the relative allele frequency range spans 0.5, both alleles were included for some SNPs.

A custom Python program (see URLs section below) generated using PyEvolve version 0.89.9 (ref. 16) was used to calculate the length of complete homozygosity (LCH) for each of the alleles in the matched set for both CEU and ASN, using the total HapMap data set, excluding monomorphic SNPs. The algorithm identified individuals who are homozygous for each target allele and determined the length of the largest region spanning the target SNP in which all these individuals are homozygous for the same allele at all other SNPs; this distance was defined as the LCH.

In the ASN cohort, the LCH for the 577X allele was interrupted by a single heterozygous genotype at rs597626 in sample NA18612; we re-genotyped this individual and found this to be a genotyping error in the HapMap database. An error report has been submitted to HapMap.

For **Figure 3b**, the fraction of recombinant chromosomes (FRC) was calculated using a previously described approach[8]. Briefly, the complete HapMap genotype data set for a 750-kb region centered on R577X was downloaded, and individuals were separated by R577X genotype. Heterozygotes were discarded, and individuals homozygous for the alleles encoding Arg577 ('577RR individuals') and individuals homozygous for the alleles encoding the stop codon ('577XX individuals') were analyzed separately. If

no recombination had occurred between R577X and a target SNP in the region, that SNP was monomorphic in individuals homozygous for one allele of R577X (that is, FRC = 0). If recombination had occurred, the minor allele frequency of the target SNP in individuals homozygous for one allele of R577X served as an estimate for the FRC.

Ages of the selective sweeps in the CEU and ASN cohorts were estimated using a recently described method[9] based on the extent of decay of LD associated with the 577X allele. These estimates should be regarded as tentative, as they rely on a number of assumptions of uncertain validity[9].

Analysis of *CTSF*, *BBS1* and *ZDHHC24* genes. To minimize the possibility that the true target of selection in this region was a functional variant outside of *ACTN3*, we sequenced all coding exons of the *CTSF*, *BBS1* and *ZDHHC24* genes contained within the regions of LCH overlapping between CEU and ASN, along with >50 bp of flanking intronic sequence for each exon, in six individuals selected to represent homozygotes for each of the three major haplogroups from both the CEU and ASN cohorts. Primers used are listed in **Supplementary Table 2**. We also genotyped the only two reported nonsynonymous polymorphisms in the *CTSF* gene (rs11550508 and rs28464796) in 13 RR individuals and 17 XX individuals from our sequenced CEU and ASN cohorts, using direct sequencing or RFLP assays (**Supplementary Methods**).

Accession numbers. dbSNP: rs1815739 (R577X polymorphism).

URLs. Code for the custom Python program is available at http://jcsmr.anu.edu.au/org/dmb/compgen/software.

Note: Supplementary information is available on the Nature Genetics website.

ACKNOWLEDGMENTS

We thank T. Henwood (Children's Hospital at Westmead) for NADH and SDH staining. Antibodies to the α-actinins were provided by A. Beggs (Children's Hospital Boston). Antibody 10F5 was provided by J. Hoh (Univ. Sydney). This project was funded in part by a grant (301950) from the Australian National Health and Medical Research Council. D.G.M. and J.T.S. were supported by Australian Postgraduate Awards.

AUTHOR CONTRIBUTIONS

D.G.M., N.Y., J.W.H., F.A.L. and P.W.G. generated the knockout mouse; D.G.M., J.T.S., K.G.Q., J.M.R., N.Y., M.R.E., Y.B., A.J.K. and E.C.H. analyzed the knockout mouse phenotype; D.G.M., J.M.R., G.A.H. and S.E. performed the evolutionary analysis; D.G.M. and K.N.N. designed the studies and wrote the paper.

COMPETING INTERESTS STATEMENT

The authors declare competing financial interests: details accompany the full-text HTML version of the paper at http://www.nature.com/naturegenetics/.

Published online at http://www.nature.com/naturegenetics
Reprints and permissions information is available online at http://npg.nature.com/reprintsandpermissions

1. Mills, M. *et al.* Differential expression of the actin-binding proteins, α-actinin-2 and -3, in different species: implications for the evolution of functional redundancy. *Hum. Mol. Genet.* **10**, 1335–1346 (2001).
2. North, K.N. *et al.* A common nonsense mutation results in α-actinin-3 deficiency in the general population. *Nat. Genet.* **21**, 353–354 (1999).
3. Yang, N. *et al. ACTN3* genotype is associated with human elite athletic performance. *Am. J. Hum. Genet.* **73**, 627–631 (2003).
4. Niemi, A.K. & Majamaa, K. Mitochondrial DNA and ACTN3 genotypes in Finnish elite endurance and sprint athletes. *Eur. J. Hum. Genet.* **13**, 965–969 (2005).
5. Clarkson, P.M. *et al.* ACTN3 genotype is associated with increases in muscle strength in response to resistance training in women. *J. Appl. Physiol.* **99**, 154–163 (2005).
6. Moran, C.N. *et al.* Association analysis of the *ACTN3* R577X polymorphism and complex quantitative body composition and performance phenotypes in adolescent Greeks. *Eur. J. Hum. Genet.* **15**, 88–93 (2007).
7. The International HapMap Consortium. The International HapMap Project. *Nature* **426**, 789–796 (2003).
8. Wang, E.T., Kodama, G., Baldi, P. & Moyzis, R.K. Global landscape of recent inferred Darwinian selection for *Homo sapiens*. *Proc. Natl. Acad. Sci. USA* **103**, 135–140 (2006).
9. Voight, B.F., Kudaravalli, S., Wen, X. & Pritchard, J.K. A map of recent positive selection in the human genome. *PLoS Biol.* **4**, e72 (2006).
10. Jones, K.J. *et al.* Deficiency of the syntrophins and α-dystrobrevin in patients with inherited myopathy. *Neuromuscul. Disord.* **13**, 456–467 (2003).
11. Cooper, S.T., Lo, H.P. & North, K.N. Single section Western blot: Improving the molecular diagnosis of the muscular dystrophies. *Neurology* **61**, 93–97 (2003).
12. Reichmann, H., Srihari, T. & Pette, D. Ipsi- and contralateral fiber transformations by cross-reinnervation. A principle of symmetry. *Pflugers Arch.* **397**, 202–208 (1983).
13. Srere, P.A. Citrate synthase. *Methods Enzymol.* **13**, 3–11 (1969).
14. Koch, L.G. & Britton, S.L. Artificial selection for intrinsic aerobic endurance running capacity in rats. *Physiol. Genomics* **5**, 45–52 (2001).
15. Kong, A. *et al.* A high-resolution recombination map of the human genome. *Nat. Genet.* **31**, 241–247 (2002).
16. Knight, R. *et al.* PyCogent: a toolkit for making sense from sequence. *Genome Biol.* **8**, R171 (2007).